C1XS results - First measurement of enhanced Sodium on the Lunar surface

Athiray, P. S.; Narendranath, S.; Sreekumar, P.; Grande, Manuel

Published in:
Planetary and Space Science

DOI:
10.1016/j.pss.2014.10.010

Publication date:
2014

Citation for published version (APA):
Athiray, P. S., Narendranath, S., Sreekumar, P., & Grande, M. (2014). C1XS results - First measurement of enhanced Sodium on the Lunar surface. *Planetary and Space Science*, *104*(Part B), 279-287. https://doi.org/10.1016/j.pss.2014.10.010

Author's Accepted Manuscript

www.elsevier.com/locate/pss

C1XS results - First measurement of enhanced Sodium on the Lunar surface

P.S. Athiray, S. Narendranath, P. Sreekumar, M. Grande

PII: S0032-0633(14)00323-7
DOI: http://dx.doi.org/10.1016/j.pss.2014.10.010
Reference: PSS3836

To appear in: *Planetary and Space Science*

Received date: 19 April 2014
Revised date: 14 October 2014
Accepted date: 17 October 2014

Cite this article as: P.S. Athiray, S. Narendranath, P. Sreekumar, M. Grande, C1XS results - First measurement of enhanced Sodium on the Lunar surface, *Planetary and Space Science,* http://dx.doi.org/10.1016/j.pss.2014.10.010

C1XS results - First measurement of enhanced Sodium on the Lunar surface

P.S. Athiray[a,b,**], S. Narendranath[a], P. Sreekumar[c], M. Grande[d]

[a] *ISRO Satellite Centre, Vimanapura P.O., Bangalore 560 017, India*
[b] *Department of Physics, University of Calicut, Thenjippalam, Kerala, India*
[c] *Indian Institute of Astrophysics, Koramangala, Bangalore, India*
[d] *Institute of Mathematics, Physics and Computer Science, Aberystwyth University, UK*

Abstract

We describe the first unambiguous evidence of enhanced Sodium on the lunar surface revealed by the Chandrayaan-1 X-ray Spectrometer (C1XS). The C1XS onboard the Chandrayaan-1 spacecraft was designed to map the surface elemental chemistry of the Moon using the X-ray fluorescence (XRF) technique. During the nine months of remote sensing observations (Nov'2008 - Aug'2009), C1XS measured XRF emission from the Moon under several solar flare conditions. A summary of entire C1XS observations and data selection methods are presented. Surface elemental abundances of major rock-forming elements viz., Mg, Al, Si and Ca as well as Na derived from C1XS data corresponding to certain nearside regions of the Moon are reported here. We also present a detailed description of the analysis techniques including derivation of XRF line fluxes and conversion to elemental abundances. The derived abundances of Na (2-3 wt%) are significantly higher than what has been known from earlier studies. We compare the surface chemistry of C1XS observed regions with the highly silicic compositions (intermediate plagioclase) measured by the Diviner Radiometer instrument onboard Lunar Reconnaissance Orbiter(LRO) in those regions.

Keywords: X-ray Fluorescence(XRF), Chandrayaan-1, C1XS, lunar surface chemistry

1. Introduction

Study of lunar surface chemistry is essential in understanding the formation and evolution of lunar crust and interior under different geochemical processes on the Moon. The lunar surface has been explored extensively through returned samples from the Apollo and Luna missions and through orbital remote sensing measurements in multi-wavelengths. Since different elements undergo different geochemical processes, the lunar surface chemistry is generally studied from the observation of major types of minerals on the Moon. Surface mineralogy is inferred through visible and near-Infrared (IR) spectroscopy. High resolution global lunar mineral maps are available from various instruments such as the Ultraviolet-Visible (UV/VIS) multispectral camera and Near IR camera on Clementine (Nozette et al., 1994; McEwen & Robinson, 1997), the Spectral Profiler (SP) and Multiband Imager (MI) on Kaguya (Manabu Kato et al., 2010; Ohtake et al., 2008) and the HyperSpectral Imager (HySI) and Moon Mineralogical Mapper (M^3) on Chandrayaan-1 (Bhandari, 2005). Elemental abundances can be inferred indirectly from Near IR spectroscopy which is primarily sensitive only to Fe-bearing minerals. Diversity in the chemical composition of the Moon is mostly addressed using these proxy lunar mineral maps. Recently, the Diviner Lunar Radiometer experiment onboard the Lunar Reconnaissance

*Corresponding author at:
**Currently at Indian Institute of Astrophysics, Koramangala, Bangalore, India
Email address: athray@gmail.com (P.S. Athiray)

Orbiter (LRO) provided new insights to the iron-poor mineralogy of the Moon using thermal IR spectroscopy (0.3 to 400 μm) (Paige et al., 2010). Gamma-ray spectroscopy is also used to record gamma-ray spectra from rock-forming and radio-active elements (Lawrence et al., 1998).

X-ray fluorescence (XRF) spectroscopy through remote sensing has a long history in studying the chemical composition of atmosphere-free solar system bodies (*for example, Apollo 15 (1971), Apollo 16 (1972) (Adler & Gerard, 1972; Adler et al., 1973a,b), Smart-1 (2003) (Grande et al., 2003), Kaguya (2007) (Okada et al., 2008), Change-1 (2007) (Huixian et al., 2005) and Chandrayaan-1 (2008) (Grande et al., 2009) for the Moon, Near Earth Asteroid Rendezvous (NEAR) (1996) for the asteroid Eros (Trombka, 2000; Nittler et al., 2001), HAYABUSA (2003) for the asteroid 25143 Itokawa (Okada et al., 2006)*). Solar X-rays excite surface elements of these bodies to yield characteristic emission lines. X-ray remote sensing provides an unambiguous and unique identification of elements. The upper-most layer of the Moon (few 100μm thick) is covered with lunar regolith - fine pulverized grains of bedrock due to meteoritic bombardment. Interaction of soft X-rays (1 - 10 keV) incident on the surface are limited to the top few microns on the lunar surface (e.g., 2 microns for Na) in contrast to depths of centimeters to tens of centimeters for gamma-rays. Thus X-ray remote sensing provides a clean, direct and independent measure of elemental abundances which can be compared with abundances derived from other spectral techniques. We present new results from the most comprehensive analysis of data from the Chandrayaan-1 X-ray Spectrometer (C1XS) experiment during many weak solar flares.

2. Status of lunar surface chemical mapping

The majority of our current knowledge on the chemical makeup of the Moon is obtained from geochemical studies of returned lunar samples, augmented by analyses of lunar meteorite samples collected from different places on the earth. Adding to this are the direct remote sensing measurements from different missions. Remote sensing in X-rays/or gamma-rays provides the capability for direct chemical mapping of the Moon, but is limited by the quantity and quality of the data. Since the Apollo era, several lunar missions carried X-ray and gamma-ray experiments to map the elemental abundances. However, a unified cross calibrated map does not yet exist.

2.1. Gamma ray mapping

Characteristic gamma-rays are produced when high energy cosmic rays interact with the nuclei of rock-forming elements. Abundances of light major elements viz., Ca, Si, Al, Mg, O are derived indirectly due to strong dependency on neutron production as well as changes in the lunar subsurface neutron flux (Yamashita et al., 2008). Furthermore, gamma-ray data exhibit a complex and highly uncertain background arising from various sources (Zhang et al., 2012). Global maps of various rock-forming and radio-active elements are available from the Gamma Ray Spectrometer (GRS) onboard Lunar Prospector (LP) (Lawrence et al., 1998). Recently, the global distribution of Ca abundance on the Moon has been obtained from the GRS data from Kaguya (Yamashita et al., 2012). However, the accuracy of abundances from GRS data is limited since the blending of the lines and the mix of physical processes make the analysis uncertain.

2.2. X-ray mapping

The surface chemistry of the Moon can be studied from the characteristic X-ray line intensities of different elements, emitted under solar X-ray bombardment. Simultaneous measure of the incident solar X-ray spectrum is essential for deriving elemental abundances. Major dependencies such as matrix effects, geometry and elastic scattering of solar X-rays also have to be considered for precise elemental analysis. Other factors affecting the line intensity such as sample inhomogeneity and particle size distribution are difficult to characterize. XRF experiments in Apollo 15 and 16 (Adler & Gerard, 1972; Adler et al., 1973a,b) covered only 10% (Clark, 1979) of the area on the equatorial region on the nearside of the Moon and estimated relative abundances with respect to Si. Other X-ray experiments such as D-CIXS (Grande et al., 2003) onboard SMART-1 and XRS onboard Kaguya (Okada et al., 2008, 2009) suffered from severe radiation damage which restricted its ability to yield meaningful quantitative analysis. Hence there are no measures of absolute elemental abundances from any earlier X-ray experiments.

C1XS reached and observed the Moon flawlessly without losing much of its high spectral capability. Due to overall low solar activity in this period, it could not produce global elemental maps of the Moon during its short mission life of $\approx$ 9 months. Nevertheless, simultaneous observation of multiple elements were seen during a few relatively weak flares. Most interestingly, C1XS measured the direct detection of sodium from the lunar surface.

3. C1XS observations

3.1. Overview of C1XS

C1XS (Howe et al., 2009; Grande et al., 2009), onboard Chandrayaan-1, was designed to map the abundances of major rock-forming elements on the lunar surface using the XRF technique. The extended solar minimum that prevailed during the Chandrayaan-1 mission time-frame (Nov'08 - Aug'09), left C1XS with only a handful of solar flares (a few C, B and A class flares) during which quantitative analysis could be carried out. C1XS used an array of 24 Swept Charge Devices (SCDs) (Lowe et al., 2001), with each of area 1 cm^2, to record the X-ray emission with energies of 0.8 to 10 keV. Spatial resolution for a single spectral observation varies from <50 km to >1000 km depending on spacecraft altitude and integration time. Simultaneous observation of solar X-rays, in the energy range of 1.8 to 20 keV, impinging on the Moon, was obtained from the Si-PIN based X-ray Solar Monitor (XSM) (Alha et al., 2009) also onboard Chandrayaan-1. A detailed description of C1XS instrument, its observations, steps involved in data reduction and spectral extraction are given in Narendranath et al. (2011)(here onwards Paper-I).

3.2. Data selection

The light curve of the C1XS experiment for the entire mission is shown in Fig. 1. The plot shows integrated C1XS counts in the energy range 1 keV - 10 keV (red color points in Fig. 1) plotted along with GOES solar soft X-ray flux in the energy range 1.55 keV - 12.4 keV (blue color lines in Fig. 1). It is clearly seen that the solar X-ray activity was very minimal during the entire duration and was relatively active in X-rays only in the month of July 2009, in contrast to other times. After careful examination of all data, we adopted the following criteria in choosing good data from C1XS observations:

C1. Identification of useful observations corresponding to solar flares

C2. Selection of good observation intervals where the observed data are not contaminated by any sudden increase in the flux of charged particles

Many flare observations were filtered out due to contamination from charged particles. Also flares below B3 (dashed lines in Fig. 1) are not considered for analysis as lines corresponding to Ca, Ti and Fe are absent, resulting in large errors in the derived abundance values. Analysis and results of the biggest flare seen by C1XS (a C3 flare), which occurred on the 5^{th} July 2009 are published in Paper I. Results from flare observations during the early phase of the mission (12^{th} December 2008 and 10^{th} January 2009) are given by (Weider et al., 2012). Here we discuss results from flare observations made on the 4^{th}, 6^{th} and 8^{th} July 2009 (<= C1 class flares), as shown in the inset of Fig. 1b, which satisfied the aforesaid criteria. Footprints of these observations covered a large area on the nearside of the Moon (Fig. 2). The majority of these observations span over lunar southern latitudes which include the relatively young impact crater Tycho and its rays. A summary of good observation intervals chosen for analysis along with the class of flares observed and their respective locations on the Moon are given in Table 1

Table 1: Selected good observation intervals of C1XS data

Date/Time (UTC)	Class of solar flare	Description of observed region
4^{th} Jul'09 01:18:00-01:21:59	≈B3.5	• Nearside highland region - covered some portions of Tycho rays
6^{th} Jul'09 17:04:29-17:19:44	≈C1.1	• Nearside highland region - covered the crater Tycho and majority of its rays
8^{th} Jul'09 05:27:31-05:30:20	≈B4.2	• Nearside mixed region - from crater Capuanus to crater Campanus.

4. C1XS data analysis

C1XS observations can be broadly grouped into three types viz., background observations, ie., when X-ray & particle events are not observed, flare observations and observations during high fluxes of charged particles. Light curves depicting these types of observations are shown in Fig. 3. Spectral analysis of weak flare observations is severely constrained by low signals, requiring that data from multiple ground pixels be summed. This leads to coarser spatial mapping. Following are the major steps involved in spectral analysis:

1. Build background spectrum appropriate for the observation
2. Derive scattered spectrum of solar flare, reflected off the lunar surface
3. Derive X-ray line fluxes corresponding to different elements through spectral analysis
4. Convert line fluxes to elemental abundances using specially developed inversion algorithms

4.1. Background estimates

Background emission in X-rays arises from various sources (Hall et al., 2008). Apart from cosmic X-rays, interaction of high energy charged particles in lunar orbit with the instrument leads to production of X-rays which also contributes to the overall observed continuum background. The Moon encounters two major particle environments in a synodic month (29.6 days):

(a) Solar wind & high energy cosmic ray particles ($\approx$ 24 days): Continuous flux of protons and electrons with energies ranging from eV to GeV around the Moon contribute mainly to the observed steady X-ray background in C1XS.

(b) Charged particles in the Earth's geotail ($\approx$ 6 days): The geotail extends up to several hundreds of Earth radii and it primarily composed of energetic electrons with an average energy of 1 keV (increasing to several keV occasionally; (Prakash, 1975)). Sporadic release of accelerated charged particles during solar eruptive events can alter the background spectrum significantly. The accelerated charged particles travel with different speeds and reach the Earth and the Moon at different times. Spectral contamination due to bursts of charged particles is clearly identified by enhanced counts observed in the C1XS light curve (refer Fig. 3c).

The Moon was coincidentally inside the geotail when flares occurred during the 1^{st} week of July 2009. Data over a complete orbit, without particle contamination and with solar activity less than A class flare level (ie., $< 1\times10^{-8}$ W/m^2) alone are considered for background estimation.

Some of the observations made on the 6^{th} and 8^{th} July 2009 satisfied this condition and the time-averaged background X-ray spectrum used for our current analysis is shown in Fig. 4. For comparison, spectral hardening due to a sudden burst of charged particles inside the geo-tail is also shown in Fig. 4.

4.2. Scattering of solar X-rays

Background subtracted C1XS spectra contain XRF lines along with elastically scattered solar X-rays. In order to model the scattering component, the incident solar spectra for the observed C1XS timings are obtained from XSM data which was constantly observing the Sun. XSM spectral analysis is performed using the solar soft package (SSW) (Freeland & Handy, 1998) which uses solar models based on the CHIANTI5.2 (Dere et al., 1997; Landi et al., 2006) atomic database and the best fit solar parameters (ie., temperature, emission measure and coronal abundances) are obtained. The best spectral fit to one of the observed XSM spectra for a C1 class flare is shown in Fig. 5 with its spectral components. Using the best fit solar model we calculated the scattered solar component following the same approach given in Paper I (sec. 6).

4.3. XRF analysis

Detailed spectral analyses are carried out using the X-ray spectral analysis package (XSPEC) (Arnaud, 1996), where the XRF lines are modeled as Gaussian functions along with an estimated spectrum of scattered solar emission corresponding to a location/time interval (included as table model

[1]). It was noticed that the presence of a 0.4 μm thick Al filter in front of the detector could possibly contaminate and yield excess counts at 1.5 keV. Using C1XS ground calibration data (Narendranath et al., 2010), we applied a correction factor (≈ 0.15) to the detection efficiency at 1.5 keV and derived the XRF line flux of the elements. One of the best-fit C1XS spectra is shown in Fig. 7, with XRF lines indicated. Due to the relative weakness of the incident solar flares, XRF signatures of Ti & Fe are not visible in most of the observations.

Apart from lines of major rock-forming elements, C1XS has clearly observed the XRF signature of Na at $\approx$ 1.04 keV in many spectra. Earlier C1XS reports by (Narendranath et al., 2011) and (Weider et al., 2012) also discussed the detection of Na from the Moon. The former proposed the possibility of high Na content on the lunar surface, while the latter suggested that it could originate from the scattering of incident solar spectrum. XRF line fluxes of the elements, including Na (wherever observed), determined for different flare observations are compiled in Table 2.

4.4. Deriving elemental abundances

We developed an XRF inversion code *x2abundance* to convert the observed X-ray line flux to absolute elemental abundances, where a new approach is adopted using Fundamental Parameter (FP) (Criss & Birks, 1968; Rousseau & Boivin, 1998) method. A detailed description of the algorithm of *x2abundance* along with assumptions and limitations are given

[1]Table Model - A model in XSPEC can also be defined as a two column table (energy versus photon intensity at some specified binning) as opposed to an analytical form. The final model spectrum is calculated by interpolation across the bins.

by (Athiray et al., 2013a). The algorithm was validated rigorously using laboratory-based XRF experiments on metal alloys and lunar analogous rocks (Athiray et al., 2013b). Dependencies which affect XRF intensities such as the incident spectrum (I_o), matrix effects and geometry effects are all incorporated. However, the code assumes a flat, homogeneous surface which is not the case in reality. Remote sensing XRF experiments mainly sense the lunar regolith which comprises distribution of particle sizes ranging from sub-micron-sized particles to cm-sized rocks (McKay et al., 1991). The observed XRF intensity get affected by the distribution of particle size, as the mean free path of soft X-rays is smaller than the mean particle size of lunar regolith. Laboratory experiments by (Maruyama et al., 2008; N*ärä*nen et al., 2008) shows that XRF intensity decreases with increasing phase angles (angle between source-surface-detector) and increases with decreasing size of particles. However, this effect is expected to be small on C1XS results where the ground pixel dimensions are large (hundreds of km) and considers a large distribution of particle sizes (Weider et al., 2012). The effect is further minimized with the use of flux fractions (line flux/sum of the flux in all lines).

Elemental abundances along with uncertainties are determined using *x2abundance*, where the uncertainties in line flux measurements are transformed to uncertainties in abundance values following statistical methods. The abundances of Ti & Fe are kept frozen to the weighted average values derived from the C1XS C3 flare observation (5.0 wt% & 0.13 wt%) (Paper I), since they are not seen in the present spectra due to weak flare excitation. The derived elemental abundances along with 1 σ uncertainties are given in Table 3.

5. Results & Discussion

With good spectral resolution, C1XS observed XRF lines of the major rock-forming elements Mg, Al, Si and Ca from the Moon simultaneously, as well as sodium for the first time. Due to inadequate solar activity and reduced mission life C1XS could not achieve its objective of global lunar elemental mapping. However, with the best available data, we have determined the elemental abundances for the C1XS-sampled locations on the lunar surface. Through rigorous spectral analysis, we have confirmed the unambiguous detection of XRF emission of Na from the Moon. Abundances derived for the 4^{th} and 6^{th} July observations clearly exhibit lunar highland features with high Al and Ca abundances and low Mg abundances. Abundances derived for the 8^{th} July observation show high Al & Mg abundances which confirms a mixed terrain of highlands and mare.

Elemental abundances derived from the LP GRS, for a large area encompassing the C1XS-observed regions (see dashed box in Fig. 2), are compared with C1XS abundances for the same regions in Fig. 7(a). We have applied the correction factor for the Al filter to our earlier published C3 flare data and re-derived the elemental abundances, which are also included in the plot. Fig. 7(a) shows that C1XS compositions along with 1σ uncertainties match well with the distribution of abundances derived from remote sensing gamma-ray observations. For comparison, Table 3 also includes the average composition of lunar soils from Apollo 16 mission (Haskin & Warren, 1991) and the average feldspathic highland terrane composition from lunar meteorites (Korotev, 2003). It is clear that the derived abundances of Na (> 1 wt%) are larger than what has been known so far (<1 wt%). Also, our results seem to suggest an inverse relation between Ca and Na abundances

Fig. 8. According to our present understanding of highland regions from the returned lunar samples and meteorite collections, there exists a strong positive correlation between Al and Ca abundances, as shown in Fig. 7(b)i (Demidova et al., 2007). The results from C1XS show a lower Ca abundance for the intervals where Na is observed and the correlation improves when Ca and Na abundances are added and compared against Al Fig. 7(b)ii.

Lunar observations & Magma Ocean Theory : Our current understanding of lunar evolution is based on the Lunar Magma Ocean (LMO) theory (Taylor, 1982; Warren, 1985, 1990) which states that the Moon was mostly/partially molten in its past. Subsequently, elemental fractionation occurred during the cooling phase of the magma. The LMO theory advocates the assumption of a global distribution of ferroan anorthosites. Ferroan anorthosites mostly consist of anorthosite rocks which are characterized by plagioclase feldspar minerals with high calcium content. It is thus assumed, that the lunar highland crust was formed from plagioclase feldspar, floating on a global magma ocean. This theory is completely based on the analysis of samples of ferroan anorthosites collected from a small area on the nearside highland region of the Moon. However, solid solutions of the plagioclase feldspar mineral group include calcic and sodic end members called anorthite ($CaAl_2Si_2O_8$) and albite ($NaAlSi_3O_8$)(Perkins, 2006). Also, different plagioclase minerals can be formed by varying the sodium/calcium content. Such minerals are considered to have intermediate plagioclase compositions. Diversity in plagioclase composition is studied by a factor called Anorthite number (An#) which is defined as $\frac{Ca}{Ca+Na+K}$ in moles. Fig. 9 shows different intermediate plagioclase minerals starting from high calcic end member to high sodic end member. Studying the diversity of plagioclase compositions in the lunar highlands is an outstanding question in lunar science eg. (Donaldson Hanna et al., 2012a). This can be addressed by mapping the distribution of anorthite content (An#) on the lunar highlands.

Global distribution of pure ferroan anorthosite (PAN) obtained from the MI and SP instruments onboard SELENE, indicated high calcic plagioclase feldspar ($>An_{95}$) (Ohtake et al., 2009) in the highland crust, in clear support of the LMO theory. It should be noted that both instruments were operated in the NIR region where plagioclase with minor amounts of iron, exhibits a broad absorption band centered around 1.25 μm owing to the electronic transitions of Fe^{2+}. But NIR spectroscopy is less sensitive to An# and hence cannot address the presence of calcic and sodic content in plagioclase feldspar.

Thermal Infrared (TIR) spectroscopy has been extensively used in the laboratory to study the variations in plagioclase minerals (Donaldson Hanna et al., 2012b) using the position of Christiansen Frequency (CF), an emissivity maximum that indicates the composition related to (An#). In silicate minerals, the emissivity maximum occurs around $8 \mu m$ when the real part of refractive index approaches unity (Pieters, 1999). Ca-rich feldspathic anorthite exhibit CF positions around 7.84 μm whereas plagioclase with Na component shift towards lower CF values ≤ 7.8 μm (Donaldson Hanna et al., 2014). Ultramafic minerals exhibit intermediate and long CF values which are indicated in the CF value map shown in Fig. 10. Using this diagnostic feature, the Diviner instrument onboard the LRO identified intermediate plagioclase compositions (Greenhagen et al., 2010; Kusuma et al., 2012) over numerous areas on the Moon which were shown to be pure plagioclase feldspar using the NIR measurements of the MI and SP instruments. Fig. 10 shows the overplot of C1XS observed regions on the LRO diviner CF value map. Some of the C1XS observed regions are likely to be dominated by the impact ejecta and disturbed regolith due to the young impact crater Tycho. It is clear that some of the regions observed by C1XS show unusual mineral compositions. The An# values derived from C1XS abundances correspond to intermediate plagioclase compositions such as labradorite and bytownite. However the LMO theory predicts alkali depletion over the whole Moon as a consequence of the moon-forming giant impact. The C1XS results indicating high Na content contradict the extreme loss of volatiles by vaporization. There exist physical processes which do not require alkali depletion of the bulk Moon (Nekvasil et al., 2013). These authors have also shown that the bulk Moon could still retain alkali-rich contents under different temperature and pressure conditions. From our observations over the impact crater Tycho and its rays, we suggest that the ejecta has excavated alkali-rich material from deep layers of the bulk Moon. Suggestive evidences are also seen in Diviner images showing unusual compositions over relatively young impact craters. The first results from the Ultraviolet-Visible Spectrometer (UVS) onboard LADEE (The Lunar Atmosphere and Dust Environment Explorer) measured spatial and temporal variations of Na flux in the exosphere (Colaprete et al., 2014). Associations with surface compositions, meteorites etc., are being examined and could pave the way for further confirmation.

6. Conclusion

To summarize, the C1XS experiment performed extremely well and proved its capability by distinctly observing XRF lines of rock-forming elements from the Moon. In this paper, we have presented a detailed description of the entire C1XS observation data. Due to lack of confidence, earlier quantitative elemental estimates for certain selected flare observations (5^{th} Jul'09, 12^{th} Dec'08 & 10^{th} Jan'09) made by (Narendranath et al., 2011; Weider et al., 2012) did not include Na. Based on the selection criteria and spectral analysis steps described here, we clearly showed the unambiguous direct detection of Na from the Moon. Further, we also determined the elemental abundances, including Na for the first time, for additional flare observations on the 4^{th}, 6^{th} & 8^{th} Jul'09. The derived abundances of sodium are significantly larger than what has been known from earlier studies of lunar materials. The compositions determined from C1XS tend to support recent theories and findings of intermediate plagioclase on the Moon. However, precise Ca and Na abundance measurements are required on a global scale to address the evolution of the lunar surface. In this regard, the qualitative and quantitative study of Na abundance by X-rays will be one of the prime science objectives of the CLASS instrument on India's upcoming second mission to the Moon, Chandrayaan-2.

7. Acknowledgments

We thank the anonymous referee whose edits and suggestions greatly improved the paper.

Adler, I. et al., 1973. Results of the Apollo 15 and 16 X-ray experiment. Geochim. Cosmochim. Acta, 3, 2783-2801.

Adler, I. et al., 1973. Apollo 15 and 16 results of the integrated geochemical experiment. The Moon, 7, 487-504

Adler, I., Gerard, J., 1972. The Apollo 15 X-ray fluorescence experiment. Geochim. Cosmochim. Acta, 3, 2157-2178

Alha, L. et al., 2009. Ground calibration of the Chandrayaan-1 X-ray Solar Monitor (XSM). Nucl. Instr. Meth. A, 607, 544-553.

Arnaud, K.A., 1996. XSPEC: The first ten years. ASP Conf. Ser. 101, 170-20.

Athiray, P. S. et al., 2013a. Validation of methodology to derive elemental abundances from X-ray observations on Chandrayaan-1, Planet. Space Sci., 75, 188-194.

Athiray, P. S. et al., 2013b. Experimental validation of XRF inversion code for Chandrayaan-1, Planet. Space Sci., 89, 183-187.

Bhandari, N, 2005. Chandrayaan-1: Science goals, J. Earth system Sci., 114, 701-709.

Pieters, 1999. Lunar materials from the visible to mid-infrared : The effects of space weathering. Planetary petrology and geochemistry, 243 - 250.

Clark, P.E., 1979. Correction, Correlation and Theoretical Intensity Consideration of Lunar X-ray Fluorescence Intensity Ratios. PhD thesis. University of Maryland, Maryland, USA

Colaprete, A. et al., 2014. Overview of the LADEE Ultraviolet-Visible Spectrometer: Design, Operations and Initial results. 45^{th} Conference on the Lunar and Planet. Sci., 2566.

Criss, J.W., Birks, L.S., 1968. Calculation methods for fluorescent X-ray Spectrometry: Empirical coefficients vs fundamental parameters. Anal. Chem., 40, 1080-1088.

Demidova, S. I. et al., 2007. Chemical composition of lunar meteorites and the lunar crust. Petrology, 15, 386-407.

Dere, K. P., et al., 1997. CHIANTI - An atomic database for emission lines. Astron. Astrophys., 129, 149-173.

Dexter Perkins, Mineralogy, Second Edition, Pearson Prentice Hall. (2006).

Donaldson Hanna, K.L. et al., 2014. Global assessment of pure crystalline plagioclase across the Moon and implications for the evolution of the primary crust, J. Geophys.

Res. Planets, 119, 1516-1545.

Donaldson Hanna, K. L. et al., 2012a. Compositional diversity of crystalline plagioclase in the lunar highlands. 2^{nd} Conference on the Lunar Highlands Crust , 9024.

Donaldson Hanna, K.L. et al., 2012b. Laboratory emissivity measurements of the plagioclase solid solution series under varying environmental conditions. J. Geophys. Res. Planets, 117, E11004.

Freeland, S. L., and Handy, B. N., 1998. Data analysis with the solar soft system. Sol. Phys., 182, 497-500

Grande, M., et al., 2009. The C1XS X-ray Spectrometer on Chandrayaan-1. Planet. Space Sci., 57, 717-724.

Grande, M., et al., 2003. The D-CIXS X-ray mapping spectrometer on SMART-1. Planet. Space Sci., 51, 427-433.

Greenhagen, B. T. et al., 2010. Global Silicate Mineralogy of the Moon from the Diviner Lunar Radiometer. Science, 329, 1507-1509.

Hall, D. et al., 2008. Simulating and reproducing instrument background for X-ray CCD spectrometers in space. Proc. SPIE, 7021, 58-69.

Howe, C. J., et al., 2009. Chandrayaan-1 X-ray Spectrometer (C1XS) instrument design & technical details. Planet. Space Sci., 57, 735-743.

Korotev, L. R. et al., 2003. Feldspathic lunar meteorites and their implications for compositional remote sensing of the lunar surface and the composition of the lunar crust. Geochim. Cosmochim. Acta, 667, 4895-4923.

Kusuma, K. N. et al., 2012. Geochemical and mineralogical analysis of Gruithuisen region on Moon using M3 and DIVINER images., Planet. Sp. Sci., 67, 46-56.

Landi, E. et al., 2006. CHIANTI - An atomic database for emission lines VII: New data for X-rays and other improvements. Astrophys. J., 162, 261-280.

Larry Haskin and Paul Warren, 1991. Lunar Chemistry, Lunar Source Book, p 357-474.

Huixian et al., 2005. Scientific objectives and payloads of Chang'E-1 lunar satellite. J. Earth Sys. Sci. 114, 789.

Larry R. Nittler., et al., 2001. X-ray fluorescence measurements of the surface elemental composition of asteroid 433 Eros. Met. Plan. Sci., 36, 1673-1695.

Lawrence, D.J. et al., 1998. Global elemental maps of the Moon: The Lunar Prospector

gamma-ray spectrometer. Science, 281, 1484-1489.
Lowe, B. G., et al., 2001. The swept charge device, a novel CCD-based EDX detector: First results. Nucl. Instr. Meth. A, 458, 568-579.
Lucey, G. P., 1998. Model near-infrared optical constants of olivine and pyroxene as a function of iron content. J. Geophys. Res. 103, 1703-1713.
Manabu Kato et al., 2010. The Kaguya Mission Overview. Sp. Sci. Rev. 154, 3-19.
Maruyama, Y., et al., 2008. Laboratory experiments of particle size effect in X-ray fluorescence and implications to remote X-ray spectrometry of lunar regolith surface. Ear. Planets Space, 60, 293-297.
McKay, D. S., et al., 1991. Lunar Source Book: A Users Guide to the Moon. Cambridge Univ. Press, pp. 285-356.
McEwen, A.S. and Robinson. M, 1997. Mapping of the Moon by Clementine. Adv. Sp. Res. 19, 1523-1533.
*Närä*nen, J. et al., 2008. Laboratory studies into the effect of regolith on planetary X-ray fluorescence spectroscopy. Icarus, 198, 408-419.
Narendranath, S. et al., 2010. Calibration of the C1XS Instrument on Chandrayaan-1. Nucl. Instr. Meth. A, 621, 344-353.
Narendranath, S. et al., 2011. Lunar X-ray fluorescence observations by the Chandrayaan-1 X-ray Spectrometer (C1XS): Results from the nearside southern highlands. ICARUS, 214, 53-66.
Nekvasil, H. et al., 2013. Alkali depletion of the bulk Moon, Is it required?. Proc. Lunar Planet. Sci. Conf., 44, 2830.
Nozette, S. et al., 1994. The Clementine Mission to the Moon - Scientific Overview. Science 266, 1835-1839
Ohtake, M. et al., 2008. Performance and scientific objectives of the SELENE (KAGUYA) Multiband Imager. Earth Planets Space 60, 257-264.
Ohtake, M. et al., 2009. The global distribution of pure anorthosite on the Moon. Nature, 461, 236-241.
Okada, T. et al., 2006. X-ray fluorescence spectrometry of Asteroid Itokawa by Hayabusa. Science 312, 1338134 orbiter. Earth Plan. Space, 60, 277-281.
Okada, T. et al., 2008. Instrumentation and performance evaluation of the XRRS on

SELENE orbiter. Earth Plan. Space, 60, 277-281.

Okada, T. et al., 2009. X-ray fluorescence spectrometer (XRS) on kaguya: Current status and results. Proc. Lunar Planet. Sci. Conf., 40, 1897.

Paige, D. A. et al., 2010. The Lunar Reconnaissance Orbiter Diviner Lunar Radiometer Experiment. Space Sci. Rev., 150, 125-160.

Prakash, A. 1975, Magnetospheric protons and electrons encountered by the Moon in the plasma sheet. The Moon, 14, 71-78.

Prettyman, T. H. et al., 2006. Elemental composition of the lunar surface: Analysis of gamma ray spectroscopy data from Lunar Prospector, J. Geophys. Res. 111, 12007-12048.

Rousseau, R., Boivin, J., 1998. The fundamental algorithm: A natural extension of Sherman equation. The Rigaku J., 15, 13-28.

Taylor, S. R., 1982. Planetary Science: A Lunar Perspective (Lunar and Planetary Institute).

Trombka, J. I., 2000. he elemental composition of Asteroid 433 Eros: Results of the NEAR-Shoemaker X-ray Spectrometer, Sci., 289, 2101-2105.

Warren, P. H., 1985. The Magma Ocean Concept and Lunar Evolution. Ann. Rev. Ear. Pla. Sciences, 13, 201-240.

Warren, P. H., 1990. Lunar anorthosites and the magma-ocean plagioclase-flotation hypotheses: importance of FeO enrichment in the parent magma. Am. Mineral, 75, 46-58.

Weider, S. Z., et al., 2012. The Chandrayaan-1 X-ray Spectrometer : First results. Planet. Space Sci., 60, 217-228.

Yamashita, N. et al., 2008. Complexities of gamma-ray line intensities from the lunar surface. Earth Planet Sp., 60, 313-319.

Yamashita, N. et al., 2012. The global distribution of calcium on the Moon : Implications for high-Ca pyroxene in the eastern mare region. Earth and Planet. Sci., Let., 353, 93-98.

Zhang Liyan, et al., 2012. Background deduction of the Chang'E-1 gamma-ray spectrometer data. Chinese J. Geochem. 31, 234-241.

Table 2: X-ray line flux (photons/cm^2/s) from C1XS spectral analysis with 1σ errors. Approximate central co-ordinates of each ground pixel are given in the first column

Lat , Lon	**Date Time in UTC**	**Na Kα**	**Mg Kα**	**Al Kα**	**Si Kα**	**Ca Kα**
-45.2 , 25.0	04/07/09	-	0.54 ±	1.03 ±	0.83 ±	0.08 ±
	01:18:00 -01:21:59	-	0.06	0.08	0.06	0.01
-30.2 , 25.0	04/07/09	0.72 ±	0.83 ±	1.59 ±	1.06 ±	0.06 ±
	01:22:00 - 01:27:09	0.15	0.07	0.09	0.06	0.01
-63.2 , -10.5	06/07/09	-	0.92 ±	1.54 ±	0.94 ±	0.18 ±
	17:04:29 - 17:06:26	-	0.07	0.07	0.05	0.02
-53.2 , -10.5	06/07/09	0.56 ±	1.26 ±	2.10 ±	1.46 ±	0.12 ±
	17:06:27 - 17:10:17	0.13	0.17	0.11	0.07	0.01
-43.0 , -10.5	06/07/09	0.73 ±	1.30 ±	2.08 ±	1.31 ±	0.04 ±
	17:10:47 - 17:13:59	0.16	0.10	0.13	0.09	0.01
-30.7 , -10.3	06/07/09	-	0.88 ±	1.40 ±	1.08 ±	0.02 ±
	17:14:11 - 17:19:44	-	0.15	0.06	0.05	0.01
-30.0 , -28.7	08/07/09	0.45 ±	0.73 ±	0.92 ±	0.42 ±	0.03 ±
	05:27:31 - 05:30:20	0.22	0.05	0.04	0.02	0.01

Table 3: Elemental abundances (wt%) from C1XS analysis with 1 σ uncertainties

Lat , Lon	**Na**	**Mg**	**Al**	**Si**	**Ca**
-45.2 , 25.0	-	$4\,^{+1}_{-1}$	$16\,^{+1}_{-1}$	$18\,^{+1}_{-1}$	$13\,^{+1}_{-1}$
-30.2 , 25.0	3^{+1}_{-1}	$4\,^{+1}_{-1}$	$17\,^{+1}_{-1}$	$17\,^{+1}_{-1}$	$10\,^{+1}_{-1}$
-63.2 , -10.5	-	$6\,^{+1}_{-1}$	$18\,^{+1}_{-1}$	$13\,^{+1}_{-1}$	$14\,^{+1}_{-1}$
-53.2 , -10.5	$2\,^{+1}_{-1}$	$6\,^{+1}_{-1}$	$17\,^{+1}_{-1}$	$16\,^{+1}_{-1}$	$10\,^{+1}_{-1}$
-43.0 , -10.5	$3\,^{+1}_{-1}$	$5\,^{+1}_{-1}$	17^{+1}_{-1}	$18\,^{+1}_{-1}$	$8\,^{+1}_{-1}$
-30.7 , -10.3	-	$4\,^{+2}_{-1}$	$16\,^{+2}_{-1}$	$23\,^{+3}_{-2}$	$8\,^{+2}_{-3}$
-30.0 , -28.7	$5\,^{+0}_{-1}$	$9\,^{+1}_{-2}$	$15\,^{+2}_{-2}$	$16\,^{+2}_{-1}$	$6\,^{+1}_{-1}$
Average feldspathic meteorite compositions	0.26	3.26	14.92	20.89	11.65
AP16 (Soil & Regolith Breccia Average)	0.35	3.62	14.41	20.98	10.41
LP average (dashed box Fig. 2)	-	5.32	13.28	20.23	10.96

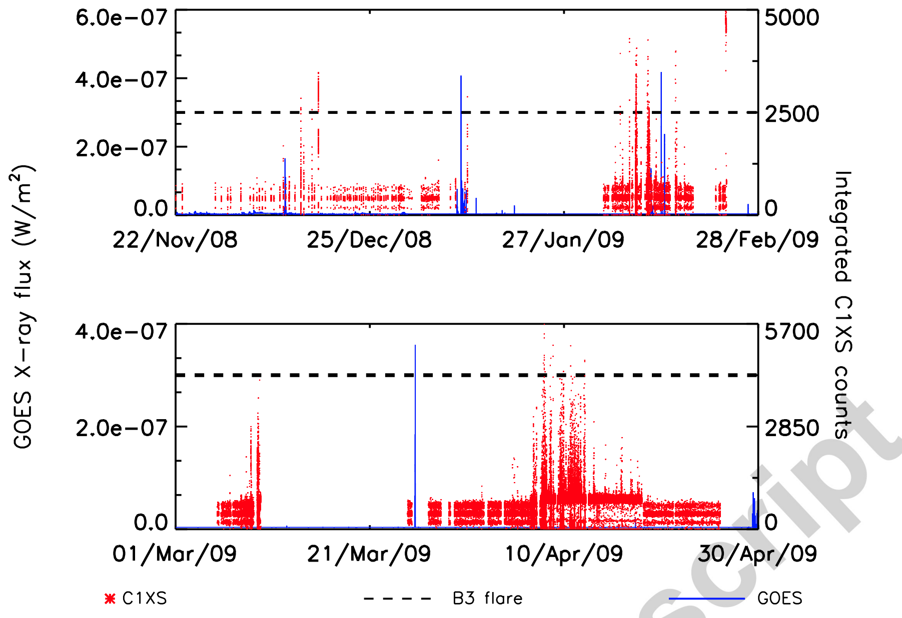

(a) Nov'2008 - Apr'2009

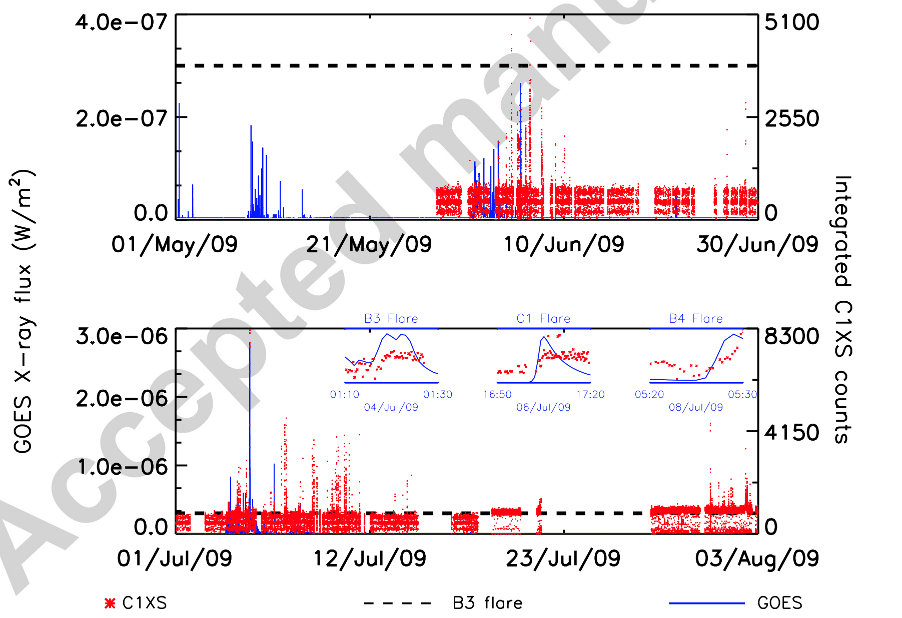

(b) May'2009 - Aug'2009

Figure 1: The entire mission light curve of C1XS experiment from 22^{nd} Nov.2008 - 3^{rd} Aug.2009. The solar soft X-ray flux from the GOES satellite indicates the X-ray activity of the Sun during the life time of the mission. Useful C1XS observations are during solar flares with intensity B3 (3×10^{-7} W/m^2) and above which is marked as dashed line. Red points indicate C1XS integrated counts with a time bin of 16s; Blue lines indicate solar X-ray flux with a time bin of 1min. Flare observations discussed in this paper are shown in the inset of Fig. 1b.

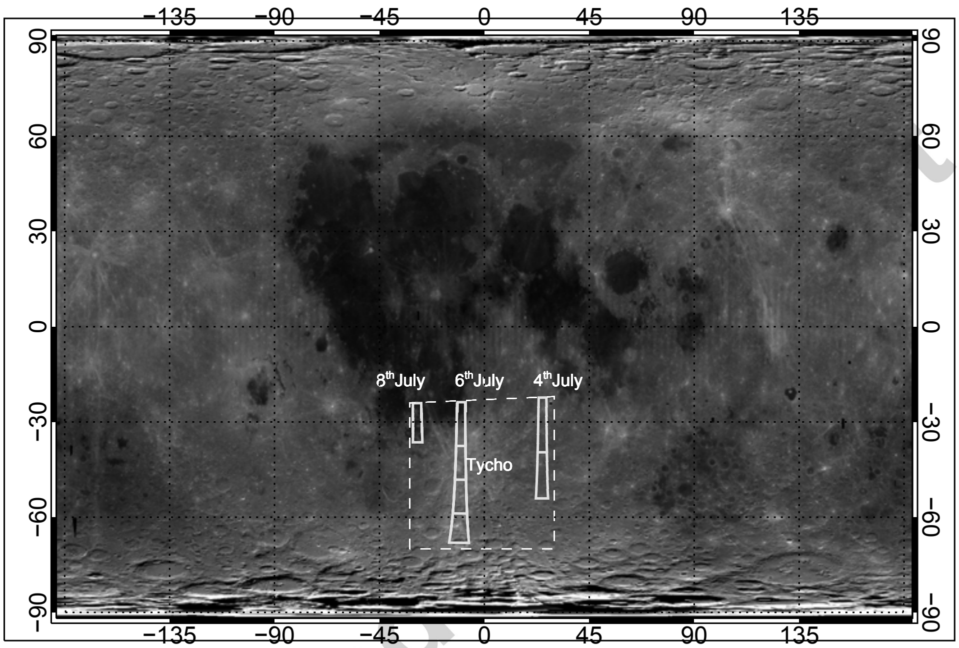

Figure 2: Ground-track of C1XS observations made on 4^{th}, 6^{th} and 8^{th} July 2009 plotted over the Clementine lunar albedo map (750nm). Elemental abundances from the LP gamma-ray data used for comparison are taken from the region of interest shown as dashed line box which encompass C1XS observed locations

.

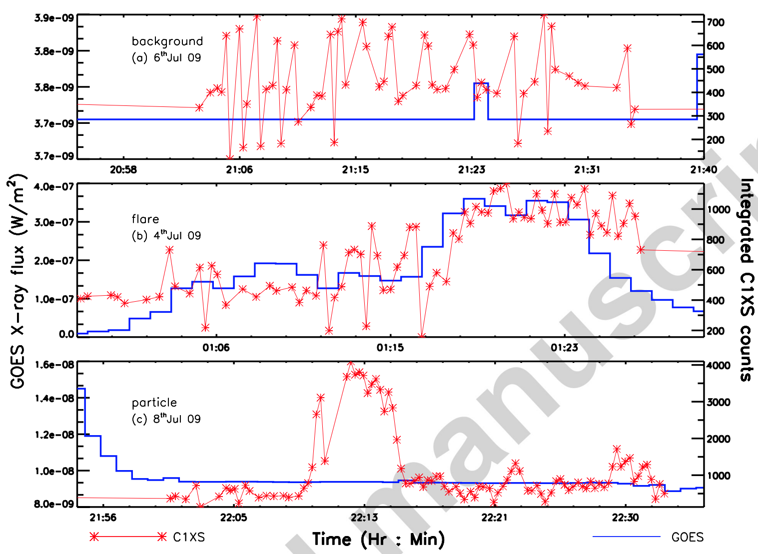

Figure 3: Light curves showing C1XS integrated counts (1 keV - 10 keV) (*Red line-points*) along with X-ray solar flux obtained from GOES (1.55 keV - 12.4 keV) (*blue lines*) (a) background observation - without solar flare and high particle flux (b) flare observation showing a rise in solar flux and C1XS counts (c) particle hit observation indicated by a sudden rise in the C1XS counts without any corresponding increase in the solar flux

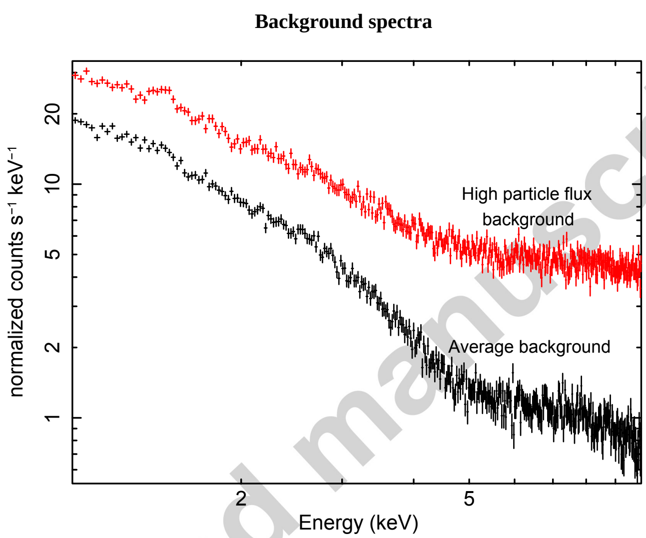

Figure 4: C1XS average background spectrum inside the geotail measured from multiple orbits during the month of July 2009 used for data analysis along with a spectrum corresponding to high particle flux (red color points).

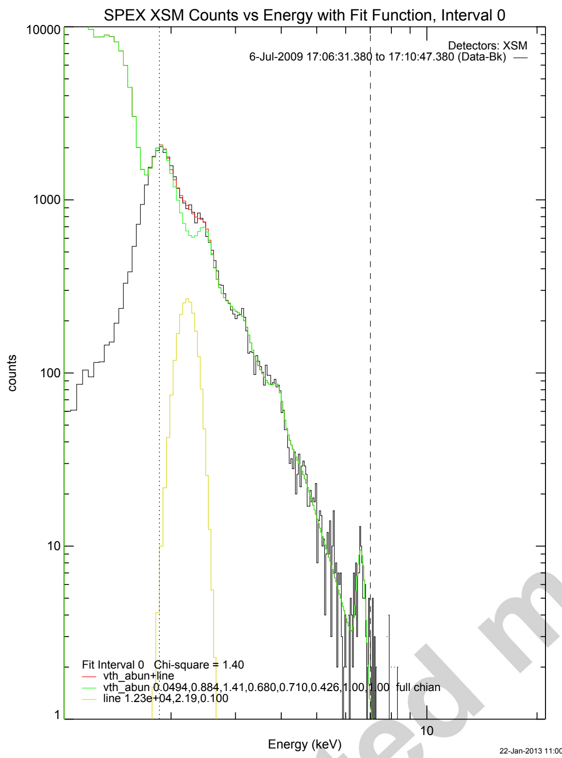

Figure 5: Best fit to one of the solar spectra observed by the XSM on 6^{th} July 2009, using the CHIANTI database. The observed continuum spectrum along with the ionized solar coronal emission lines are well modeled using *vtherm_abund* in OSPEX (Object Spectral Executive - an interface tool for solar X-ray data analysis in SSW) (Green line). Further, a Gaussian component is fitted at $\approx$ 2.1 keV (Yellow line) for improved fit. Red line represents the combined spectral fit and data points are in Black.

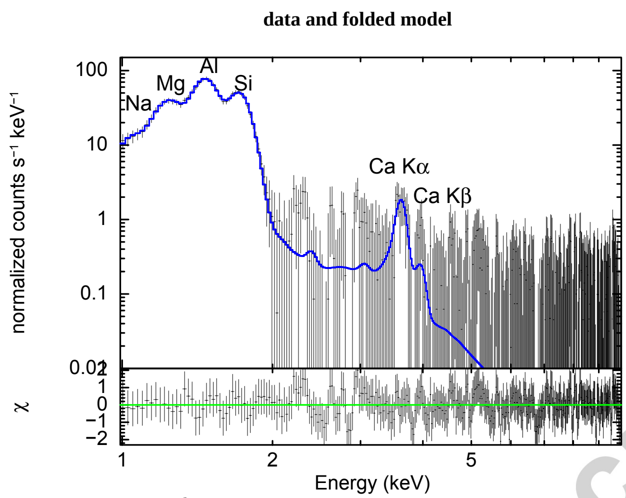

(a) 6^{th} Jul'09 - 17:10:47 - 17:13:59

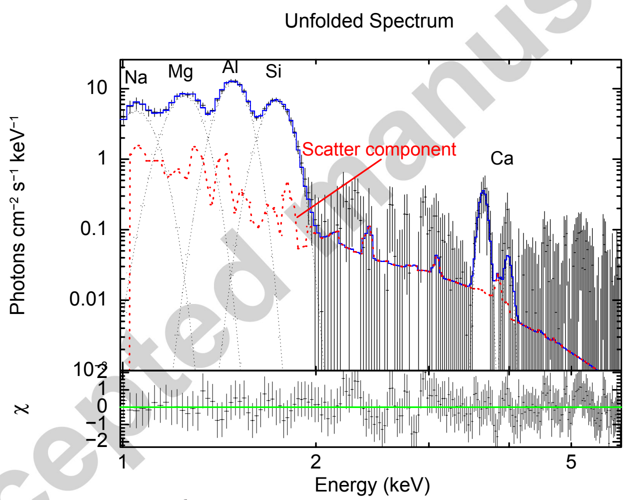

(b) 6^{th} Jul'09 - 17:10:47 - 17:13:59

Figure 6: Best fit for the observed XRF spectrum for an interval during C1 class flare, with all components. Data points (black) are shown with error bars; XRF lines of major elements are marked. Residuals of fit (difference between model and data) in terms of 1 σ error bar size are shown in the bottom panel of each figure. (a) Spectral fit convolved with detectors' response (b) Deconvolved photon spectrum corresponding to the best fit.

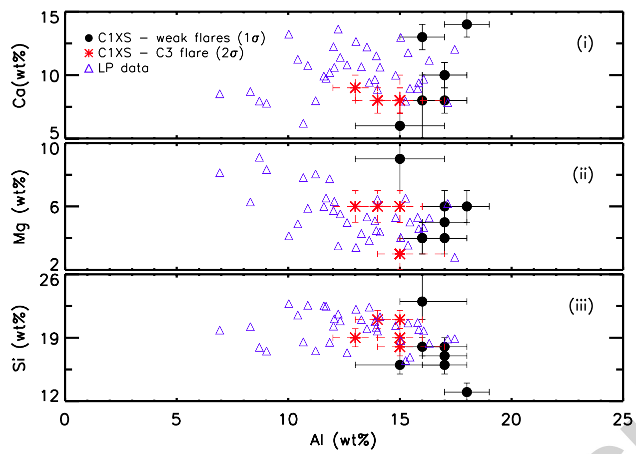

(a) C1XS abundances vs LP abundances

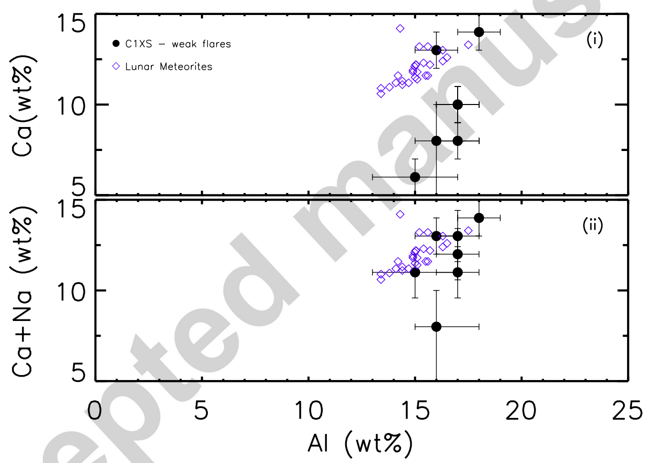

(b) C1XS abundances vs Lunar Meteorite abundances

Figure 7: Comparison of C1XS abundance with (a) GRS data from Lunar Prospector (Prettyman et al., 2006). (b) Lunar Meteorite compositions (Demidova et al., 2007). C1XS predict low Ca abundance in comparison to the correlation established between Al & Ca in lunar meteorite collections (i). Sum of Na & Ca abundances agree well with the correlation (ii).

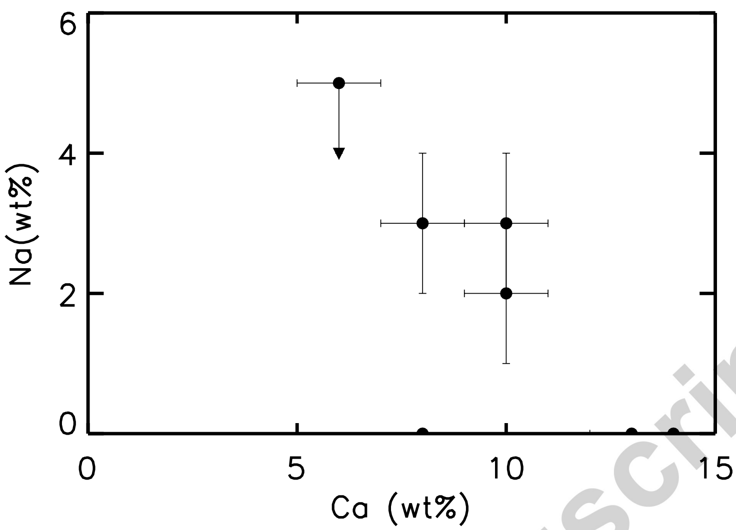

Figure 8: Relation between Ca and Na abundances from C1XS observations. The point with inverted arrow is the upper-limit of Na abundance for that observation

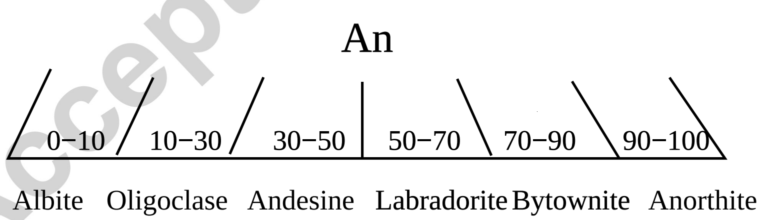

Figure 9: Plagioclase solutions from calcic end member to sodic end member which are called intermediate plagioclase minerals referred by An#.

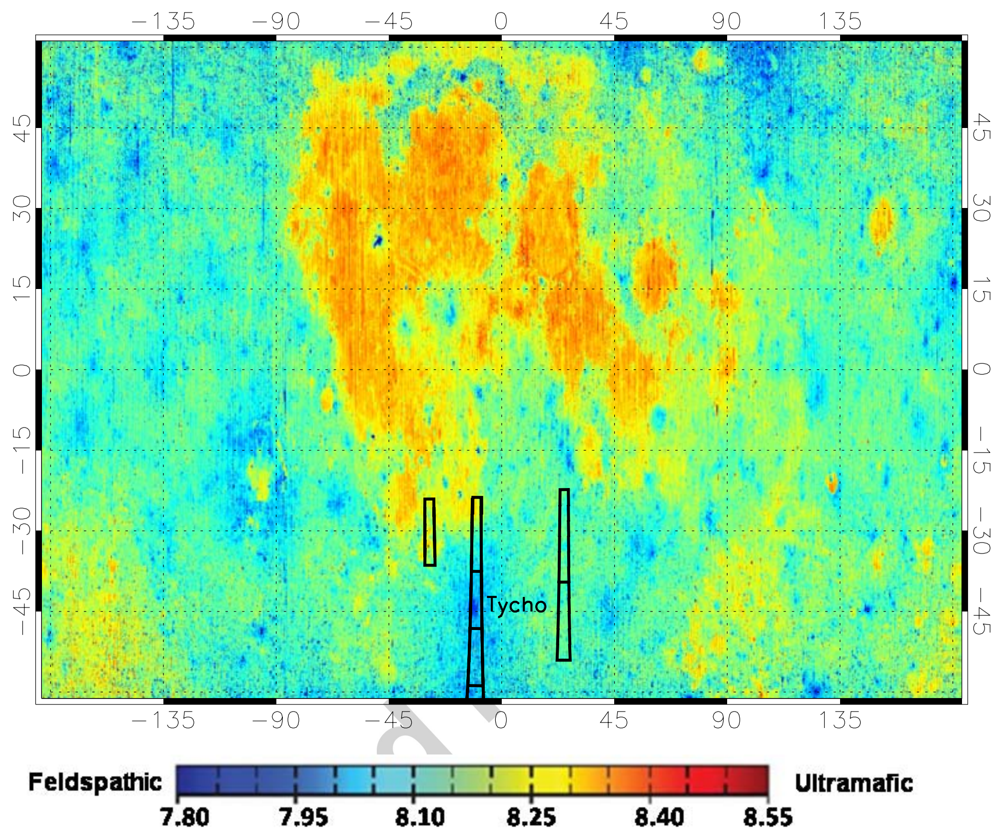

Figure 10: Track of C1XS observed region on the Moon - 4^{th}, 6^{th} and 8^{th} July 2009 plotted over the LRO Diviner radiometer Christiansen Feature (CF) value map (in μm). Ca-rich plagioclase have CF positions around 7.84 μm whereas plagioclase with Na component shift towards low CF values (leq 7.8 μm). Mafic minerals such as pyroxene, olivine show long CF values as indicated in the color map. Some of the saturate blue regions in the map with lower CF values represent unusual compositions (Greenhagen et al., 2010).